Available online at www.sciencedirect.com
ScienceDirect
International Journal of Heat and Mass Transfer 50 (2007) 3624–3637
International Journal of HEAT and MASS TRANSFER
www.elsevier.com/locate/ijhmt

Pool boiling heat transfer on horizontal rectangular fin array in saturated FC-72

Chih Kuang Yu *, Ding Chong Lu

Department of Mechanical Engineering, National Chiao Tung University, Hsin-Chu, Taiwan

Received 3 March 2006; received in revised form 22 January 2007
Available online 23 March 2007

Abstract

The flow patterns and pool boiling heat transfer performance of copper rectangular fin array surfaces immersed in saturated FC-72 were experimentally investigated. The effects of the geometry parameters (fin spacing and fin length) on boiling performance were also examined. The test surfaces were manufactured on a copper block with a base area of 10 mm × 10 mm with three fin spacing (0.5 mm, 1.0 mm and 2.0 mm) and four fin lengths (0.5 mm, 1.0 mm, 2.0 mm and 4.0 mm). All experiments were performed in the saturated state at 1 atmospheric condition. A plain surface was used as the reference standard and compared with the finned surfaces. The photographic images showed different boiling flow patterns among the test surfaces at various heat fluxes. The test results indicated that closer and higher fins yielded a greater flow resistance that against the bubble/vapor lift-off in the adjacent fins. Moreover, as the heat flux approached to critical heat flux (CHF), numerous vapor mushrooms periodically appeared and extruded from the perimeter of the fin array, causing dry-out in the center of the fin array. Closer and higher fins provide more heat transfer. The results also showed that overall heat transfer coefficient decayed rapidly as the fin spacing decreased or the fin length increased. The maximum value of CHF on the base area was 9.8×10^5 W m^{-2} for the test surface with a 0.5 mm fin spacing and a 4.0 mm fin length, which has a value five times greater than that of the plain surface.

Keywords: Pool boiling; Fin array; FC-72; Critical heat flux

1. Introduction

As the VLSI technology has advanced in the recent decades, the trend of the electronics industry has reduced chip sizes and increased the concentration of the circuits and number of transistors in a silicon chip. Advances in chip design have also increased the power dissipated in a small volume. Today's electronic components consume much power and operate at an extremely high temperature. Therefore, current heat transfer capacities must be improved to enable the thermal management of electronic components.

Boiling heat transfer is a highly efficiency technique, which provides a heat transfer coefficient that is two orders of magnitude higher than that of single phase heat transfer, proposed by Bar-Cohen [1]. However, boiling heat transfer is constrained to the nucleate boiling region by two effects – boiling hysteresis and critical heat flux. Boiling hysteresis is a delay in the incipience superheat of nucleate boiling. The heating surface is cooled continuously by natural convection and surface temperature is raised with power input until the sufficient superheat is reached to initiate boiling. High boiling incipience superheat induces the thermal stress of the material and reduces the operating life of the component. As the surface heat flux of component is reached to CHF, the component temperature rises rapidly,

* Corresponding author. Address: Rm. 168, Bldg. 14, 195, Sec. 4, Chung Hsing Road Chutung, Hsinchu, Taiwan 310, Taiwan, ROC. Tel.: +886 3 5913247; fax: +886 3 5820374.
E-mail address: Ivanckyu@itri.org.tw (C.K. Yu).

0017-9310/$ - see front matter © 2007 Elsevier Ltd. All rights reserved.
doi:10.1016/j.ijheatmasstransfer.2007.02.003

Nomenclature

A	area (m^2)
Bo	bond number
CHF	critical heat flux ($W\,m^{-2}$)
C_p	specific heat ($W\,kg^{-1}\,K^{-1}$)
D_d	bubble departure diameter (mm)
g	gravitational acceleration ($m\,s^{-2}$)
I	current (A)
i_{lv}	latent heat of vaporization ($J\,kg^{-1}$)
Ja	Jacob number
k	thermal conductivity ($W\,m^{-1}\,K^{-1}$)
L	fin length (mm)
h	heat transfer coefficient ($W\,m^{-2}\,K^{-1}$)
M	molecular weight of liquid
n	numbers of fins
Pr	Prandtl number
P_{sat}	saturation pressure (Pa)
$\dot{Q}$	heat transfer rate (W)
q''	heat flux ($W\,m^{-2}$)
R_p	surface roughness
S	fin spacing (mm)
T	temperature (K)
T_m	temperature (K)
ΔT	surface superheat (K)
V	voltage (V)
W	fin width (mm)
α	aspect ratio of the fin
σ	surface tension (Nm^{-1})
ρ	density ($kg\,m^{-3}$)

Subscripts

b	base surface area
f	finned surface
l	saturated liquid
p	plane surface
sat	base on saturation condition
t	total finned surface area
v	saturated vapor

causing the burnout of the component. Hence, reducing the boiling hysteresis and increasing the CHF will overcome the limitations on boiling heat transfer technology in electronic cooling applications.

There are several parameters which including pressure, subcooling, orientation, surface structure and extending surface area can be used to enhance the boiling heat transfer are discussed by Thome [2], especially for the boiling mechanism on enhanced surface. Bondurant and Westwater [3] and Klein and Westwater [4] experimentally analyzed transverse fins and cylindrical spins boiling in R-113 and water. The test results showed that the fins could be space as closely as 1/16 in. without causing bubble interference among fins and a closer spacing could also reduces the heat duty. Haley and Westwater [5] observed long single horizontal fin boiling in isopropyl alcohol and R-113. The results indicated that various heat transfer modes, including the stable film, transition and nucleate boiling with free convection, could occur simultaneously along a fin, revealing the extremely complex mechanism on boiling fins. Mudawar [6] investigated low-profile micro-stud boiling in FC-72 and FC-87. They used their proposed numerical analytic method for a single fin model to predict the boiling heat transfer performance of their multiple fin surfaces. However, Siman-Tov [7] found that heat transfer performance on a fin array could not be understood by analyzing a single fin. Guglielmini [8,9] studied the effects of orientation and geometrical configuration on extended surface boiling in Ht-55 and FC-72 and found that straight fin surfaces offered better boiling performance than plane surface. Their experiment also showed that, for the same surface superheat, the vertically orientated non-uniformly spaced finned surfaces provided greater heat transfer than the horizontal arrangement and that uniformly spaced finned surfaces showed slightly better boiling performance. Rainey and You [10,11] studied the plain and microporous, square pin-finned surfaces boiling in saturated FC-72, and found that pin fins caused resistance to vapor/bubble departure and longer bubble residence time, increasing the flow resistance to the approaching re-wetting liquid and causing localized dry-out near the root of the fins. Hirono [12] proposed that interference between adjacent rectangular fins could reduce the boiling heat transfer performance in the high heat flux region.

Another method, which has been studied extensively to improve pool boiling heat transfer, is small-scale surface enhancement using a variety of techniques, including surface roughening, porous metallic coatings, microporous coatings, MEMS fabrication and others. Zhang and Shoji [13] examined the physical mechanisms of the interaction between nucleation sites, and found that it was governed by three factors– hydrodynamic interaction between bubbles, thermal interaction between nucleation sites, horizontal and declining bubble coalescences. Shoji and Takagi [14] employed a single artificial cavity to analyze the nonlinear behavior and low dimensional chaos of the bubbles. Recently, Honda [15] observed silicon chips with the micro-pin-fin boiling in FC-72 and found that micro-pin-fin chip exhibited a considerably greater heat transfer. Yu et al. [16] studied boiling on silicon chips with the artificial cavities in FC-72 and found a marked increase in boiling heat transfer coefficients when artificial micro-cavities were applied to the heat surface.

The pool boiling mechanism is very complex and many factors are responsible for high heat transfer rates, including latent heat transfer, natural convection and

micro-convection. Several investigators have used visualization as a tool to observe the relative contributions of those mechanisms. Nakayama et al. [17–19] were among the first to carry out visualize boiling process on structured surfaces. The surface comprised a rectangular channel that was covered with a thin sheet with pores at a regular pitch, and the entire structure was immersed in R-11. Arshad and Thome [20] visualized similar surfaces to understand the mechanism of boiling inside the channels. Xia et al. [21] observed that boiling hysteresis attenuates in narrow channels, and first local bubble site is active on the upper part of the narrow channel.

Although, many studies have been conducted on finned surfaces and the pool boiling of dielectric fluid therefrom, however, few have addressed the bubble flow mechanism of boiling on finned surfaces. Flow characteristics and related phenomena inside fin array thus remain unclear. Therefore, this study has two main goals. The first is to observe the bubble flow mechanisms of the fin array by taking photographs. The second is to elucidate the geometry effects of the fin spacing and length of horizontal finned surfaces on pool boiling heat transfer performance.

2. Experimental apparatus

An experimental facility with FC-72 as working fluid was designed and constructed to investigate the boiling phenomenon and the heat transfer performance of horizontal rectangular fin array. Fig. 1 schematically depicts the pool boiling experimental apparatus. The test rig consists of five major parts – (1) test chamber, (2) heating module, (3) measurement and data acquisition system, (4) vacuum and degas system and (5) environmental control system.

The test chamber was used to simulate the pool boiling in saturated dielectric liquid FC-72 at atmospheric pressure

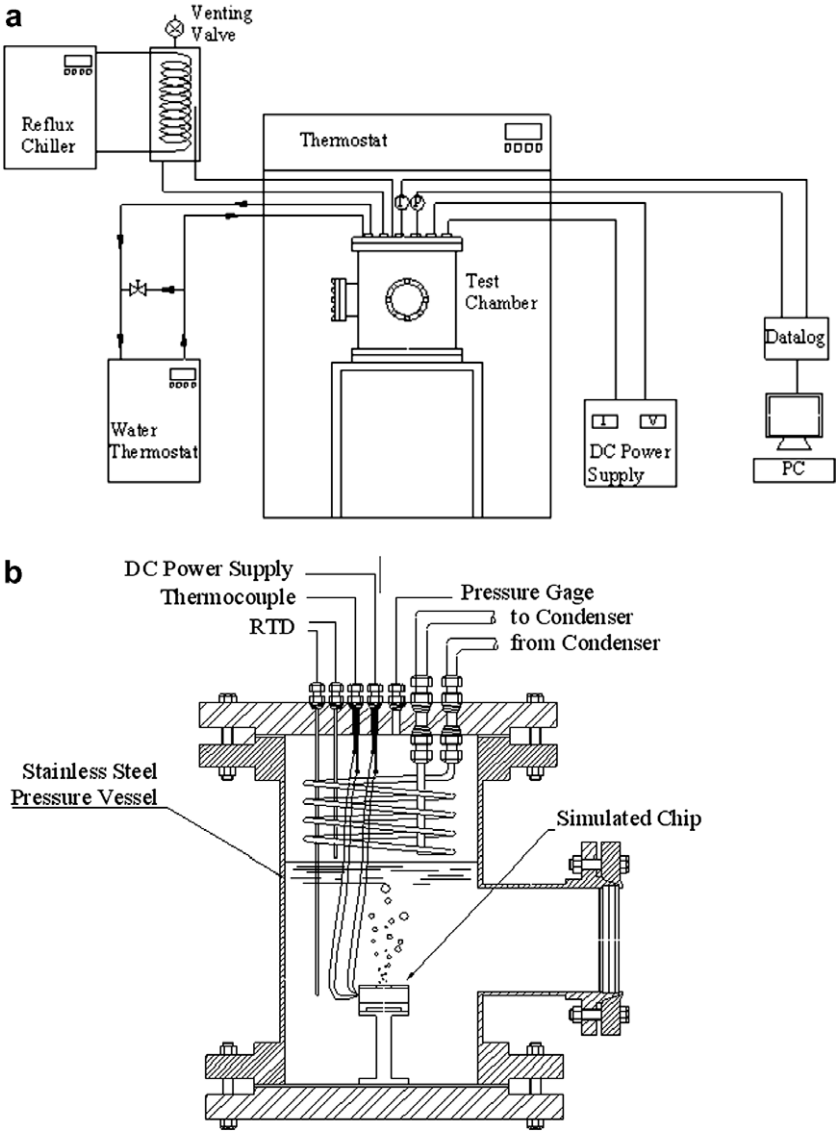

Fig. 1. Schematic of experimental apparatus: (a) major test rig and (b) test chamber.

inside a hermetic stainless steel pressure vessel, 304 mm high and 154 mm in diameter, with two quartz windows, each with a diameter of 100 mm, to enable the flow patterns of the bubbles to be visualized. The internal water condenser was coiled in the upper section inside the vessel and connected to a thermostat to keep the vessel at atmospheric pressure. A pressure transducer with an operating range of 0–4 × 10^5 Pa was also located at the gate of the vessel to measure the pool pressure. The liquid bulk temperature was measured using two RTDs with a calibrated accuracy of 0.1 K. An auxiliary cartridge heater was wrapped around the vessel to preheat the liquid bulk during the operation, and to protect against heat loss from the vessel to the ambient.

All the flanges of vessel and quartz windows are sealed by Teflon O-ring to prevent leakage. Moreover, four flange type thermocouple/power-lead feedthroughs for vacuum system are installed on upside flange of vessel to prevent leakage from the thermocouples and power-lead wire. Meanwhile, before charge FC-72 into the test chamber, the leakage test was conducted by vacuumed the vessel and then charging high pressure nitrogen (3 × 10^5 Pa). After 48 h waiting period, if the pressure variation less than 10 Pa, the vessel was considered non-leakage and experiment can be carried out.

The schematic details of the heating module are shown in Fig. 2a, which includes a test surface, a dummy heater, a bakelite frame insulator and a teflon substrate ($k \approx 0.35$ W m^{-1} K^{-1}). All test surfaces used herein were

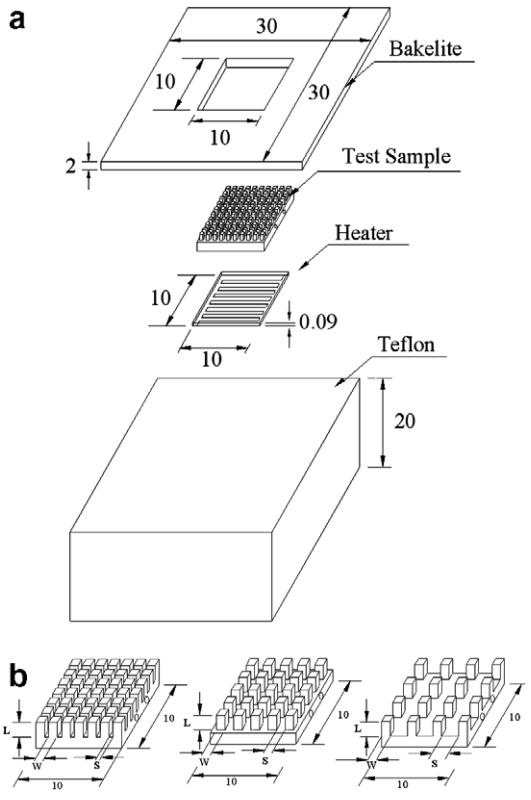

Fig. 2. Schematic of heating module and finned surfaces. (unit : mm).

Table 1
The geometry parameter of finned surfaces

A_{total}/α	$L = 0.5$ mm	$L = 1.0$ mm	$L = 2.0$ mm	$L = 4.0$ mm
$S = 0.5$ mm	198 mm^2/1	296 mm^2/2	492 mm^2/4	884 mm^2/8
$S = 1.0$ mm	150 mm^2/0.5	200 mm^2/1	300 mm^2/2	500 mm^2/4
$S = 2.0$ mm	132 mm^2/0.25	164 mm^2/0.5	228 mm^2/1	356 mm^2/2

α: aspect ratio of the fin.

manufactured from high-purity oxygen-free copper. By electrostatic discharge machining (EDM) process, the 4 × 4, 5 × 5 and 7 × 7 fin array surfaces with different fin spacing of 2 mm, 1 mm and 0.5 mm, as shown in Fig. 2b were machined from the 10 mm × 10 mm base area, with fins of width 1 mm, and 0.5, 1, 2 and 4 mm fin length respectively. The base temperatures were measured using two T-Type thermocouples which were inserted and soldered in the two holes in the copper block at a depth of 1 mm under the base surface. The detailed geometry specifications of finned surfaces are list in Table 1. The dummy heater was fabricated by standard photolithography, sputtering, electro-less plating and immersion gold deposition process on a 10 mm × 10 mm × 0.09 mm aluminum nitride heat spreader ($k \approx 170$ W m^{-1} K^{-1}). The titanium/copper heating circuit (electrical resistance ≈10 Ω) was sputtered on downward-facing surface of the heat spreader. On the upward-facing surface, titanium/copper thin film was also sputtered to be the adhesive layer. Then, the copper electro-less plating and immersion gold process were conducted on the Ti/Cu layer for soldering with test surfaces. The bakelite frame insulator and the teflon substrate were mounted with test surface to prevent side heat loss. Moreover, low thermal conductivity silicone adhesive was used to seal the crevice between test surface and bakelite to prevent boiling nucleation.

The power generated from the dummy heater was provided by a DC power supply (0–160 V, 0–5 A). The heating power, simulating the heat generated by CPU, was supplied from the DC power supply.

All the signals, including those from thermocouples, RTDs and the pressure transducer were collected and converted by the internal calibration equation in a data acquisition device, which then transmitted the converted signals through a GPIP interface to a personal computer and displayed them on screen for further operation.

A microscope with a high speed camera (Fuji S602) was installed in front of the quartz window to observe the mechanism of boiling from these test surfaces. The focus plane of the camera was adjusted on the first row fins. The diameter of the departure bubble was determined by compare with the side length of bakelite frame insulator instead of fin with or fin width because of thermal expansion of copper may results measurement deviation. The boiling images captured by the camera were stored and displayed using a PC with image-capturing software. The image was recorded and the data collected simultaneously during the experiment, to enable visual images to be compared with corresponding measurements.

3. Experimental procedures

The working liquid FC-72 was filled into the test vessel before the test run. The liquid level was maintained at approximately 80 mm above the test surface to prevent any disturbance caused by the rise in vapor to the level of liquid, which would influence the boiling test. The test vessel with the operating fluid was heated to the saturation temperature, using auxiliary cartridge heaters. As the saturation temperature was reached, the operating fluid was boiled vigorously for two hours to remove dissolved gases and any non-condensed gas before the test run.

After, the liquid had been cooled from 3 h, the data acquisition system, the environment control system and the auxiliary cartridge heater were used to control and preheat the bulk liquid until the saturated state was obtained. The difference between the measured bulk liquid temperature and the saturated temperature determined by the measured pressure was less than 0.1 K, the steady state was reached and test run initiated.

The power input was increased in small steps during the test run. The voltages across the heater and the current values converted from the DC power supply were recorded by the data acquisition system, and the power input was calculated subsequently. For each value of the power input, the steady state was assumed to be reached when the difference between the temperatures measured by the two thermocouples embedded in the test surface was less than 0.2 K in a waiting period of 120 s. In the steady state, the averaged temperature gradient between the surface and bulk liquid and the heat input were determined and recorded by the data acquisition system. Meanwhile, the flow pattern images were captured using a camera. In the high heat flux region near the point of CHF (where the heat flux is about 80–90% of CHF), the instantaneous surface temperature displayed on the screen was monitored and compared with the previous surface temperature for 60 s after each increment in power input. As the temperature difference between instantaneous surface temperature and previous surface temperature was larger than 20 K, CHF was assumed to have been reached and the power supply was shut off immediately.

After the power input had been shut off and the test surface cooled for 30 min, the power input was restarted and the heat flux raised to 70–80% of CHF for a boiling period of 30 min, to activate the nucleation sites. Then, the heat flux was increased to a value close to CHF, to initiate the boiling experiment by decreasing heat flux, according to the steps described above with decreasing the power input.

4. Heat loss estimation and experimental uncertainty

The insulators of the heating module, including the bakelite frame and the teflon substrate, cannot completely prevent heat loss. Commercial computational fluid dynamic software (Flotherm) was used to perform the thermal simulation. A detailed thermal model of the heating module was developed to examine the heat losses. The simulated heat losses were 15.5–9.3% in a heat flux range from 0.2 W cm^{-2} to 1 W cm^{-2} under the single-phase natural convection condition. The uncertainties in the experimental results, including heat flux and measured temperature, were analyzed as proposed by Kline and McClintock [22]. Table 2 summarizes the results of this uncertainty estimation.

Table 2
The uncertainty analysis of experiments

Parameter	Uncertainty
Test surface geometry	
Width of plain surface (%)	±0.5
Area of finned surface (%)	±1.0
Fin length, width, and spacing (%)	±0.5
Area of finned surface (%)	±4.0
Parameter measurement	
Temperature, T (°C)	±0.2
Temperature difference, ΔT(°C)	±0.3
System pressure, P (kPa)	±0.5
Boiling heat transfer on plain surface	
Power input, $\dot{Q}$ (%)	±9.2
Heat flux, q'' (%)	±11.8
Heat transfer coefficient, h (%)	±13.4
Boiling heat transfer on finned surface	
Power input, $\dot{Q}$ (%)	±9.2
Heat flux, q'' (%)	±14.2
Heat transfer coefficient, h (%)	±16.4

5. Data reduction

In the analysis of the boiling heat transfer performance, the overall heat transfer coefficient of the rectangular fin array was defined as

$$h_t = q''_t/\Delta T \tag{1}$$

where q''_t is the heat flux through the total area and ΔT represents the wall superheat, which can be determined by experimental measurement. The heat transfer rate was determined from output current of the DC power supply and measured voltage across the dummy heater. The heat flux can be based on either the base surface area (A_b=100 mm^2), or the total surface area (A_t, the summation of the base area and the fin area).

$$\dot{Q} = I \times V \tag{2}$$

$$q''_t = \dot{Q}/A_t \tag{3}$$

$$A_t = A_b + n \cdot (4W \cdot L) \tag{4}$$

where W is the width and L is the length of the fin.

The heat transfer inside the base of finned surface is determined as one-dimensional heat conduction

$$T_b = T_m - \dot{Q} \cdot \Delta x/k \cdot A_b \tag{5}$$

where T_m is the average measured temperature; Δx is the distance between the base surface and the thermocouple, and k is the thermal conductivity of the test surface.

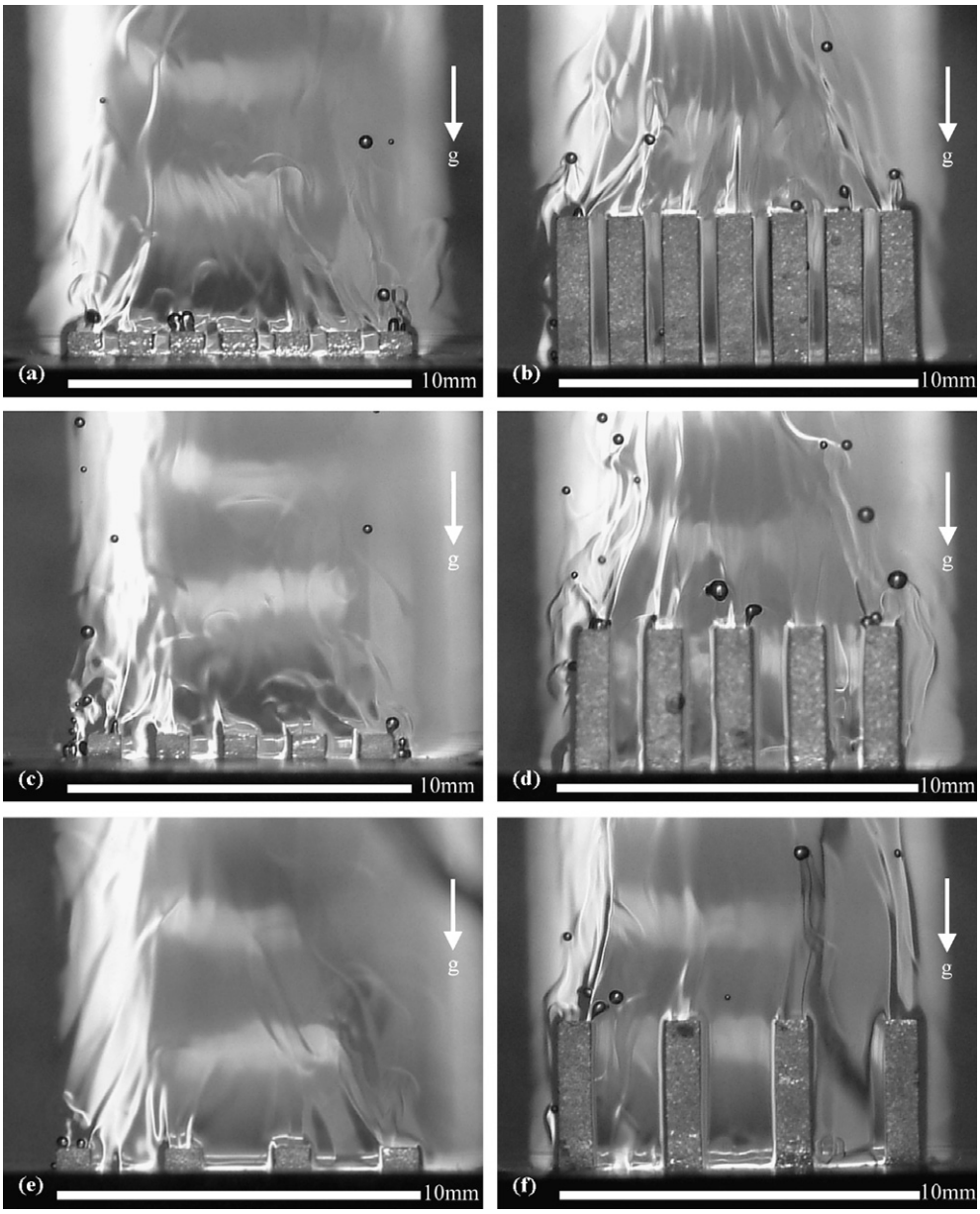

Fig. 3. Flow patterns of 6 finned surfaces at boiling incipience. (a) $S = 0.5$ mm, $L = 0.5$ mm, 2.1% of CHF; (b) $S = 0.5$ mm, $L = 4.0$ mm, 1.1% of CHF; (c) $S = 1.0$ mm, $L = 0.5$ mm, 2.3% of CHF; (d) $S = 1.0$ mm, $L = 4.0$ mm, 1.4% of CHF; (e) $S = 2.0$ mm, $L = 0.5$ mm, 2.3% of CHF and (f) $S = 2.0$ mm, $L = 4.0$ mm, 1.2% of CHF.

The wall superheat ΔT is defined as the difference between the temperature of the base surface (T_b) and the saturated temperature of FC-72 (T_{sat}).

$$\Delta T = T_b - T_{sat} \tag{6}$$

6. Results and discussion

The boiling mechanism is complex and governed by several factors, and the information of the heat transfer coefficient includes the surface temperature and input power does not suffice to elucidate boiling heat transfer associate with the finned surface. Hence, the bubbly flow pattern was observed to explore the flow mechanism and the geometry parameter effects on the boiling heat transfer performance. All tests involved FC-72 at 1 atmospheric with increasing heat flux to observe the boiling incipience wall superheat and CHF values. Tests with decreasing heat flux were also performed to examine the overall heat transfer coefficient in fully nucleate boiling region.

7. Observation of visual flow pattern on finned surface

Progressive photographic observations were used to investigate the effects of geometry parameters with the heat flux from 2×10^4 W m^{-2} to 9.5×10^5 W m^{-2}. Fig. 3 shows the flow pattern images of six finned surfaces at boiling incipience. As the boiling was initiated, the bubbles were

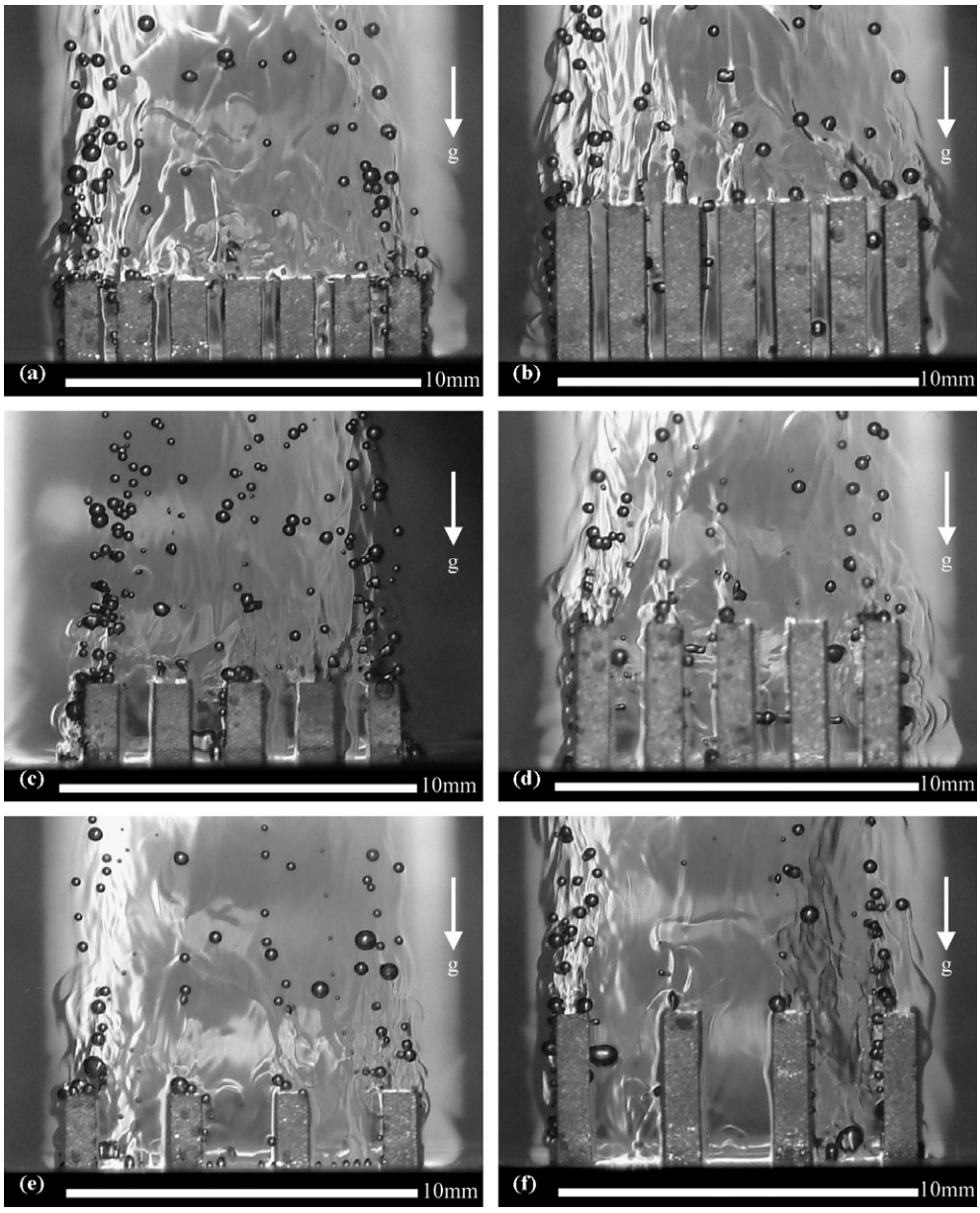

Fig. 4. Flow patterns of 6 finned surfaces at inferior heat flux regime. (a) $S = 0.5$ mm, $L = 2.0$ mm, 24.5% of CHF; (b) $S = 0.5$ mm, $L = 4.0$ mm, 23.3% of CHF; (c) $S = 1.0$ mm, $L = 2.0$ mm, 24.6% of CHF; (d) $S = 1.0$ mm, $L = 4.0$ mm, 22.1% of CHF; (e) $S = 2.0$ mm, $L = 2.0$ mm, 22.6% of CHF and (f) $S = 2.0$ mm, $L = 4.0$ mm, 23.5% of CHF.

generated from some active nucleate sites of the fins and a large portion of the test surface remains under free convection condition. An interesting phenomenon observed during this boiling process was that initial boiling occurred at some particular locations. You [11] reported a similar observation.

Another interesting phenomenon observed was that initial boiling occurs at some particular locations – typically at the fin tip, whence it spreads to the fin root, regardless of whether the wall superheat at the fin root was exceeded that at the fin tip. Unlike the bubbles that departed from the fin tip and could freely flow upward, the departure bubbles from the fin root might be easily trapped at the corner of fin root momentarily without leaving. Additionally, the induced convective motion of the fluid flow might also reduce the size of trapped bubbles.

As pointed out by Cole [23], the departure bubble diameter D_d can be expressed in terms of the Bond number Bo, as,

$$D_d = \left(\frac{Bo\sigma}{g(\rho_l - \rho_g)} \right)^{0.5} \tag{7}$$

where Bo is given by Cole [23],

$$Bo = (0.04\ Ja)^2 \tag{8}$$

and

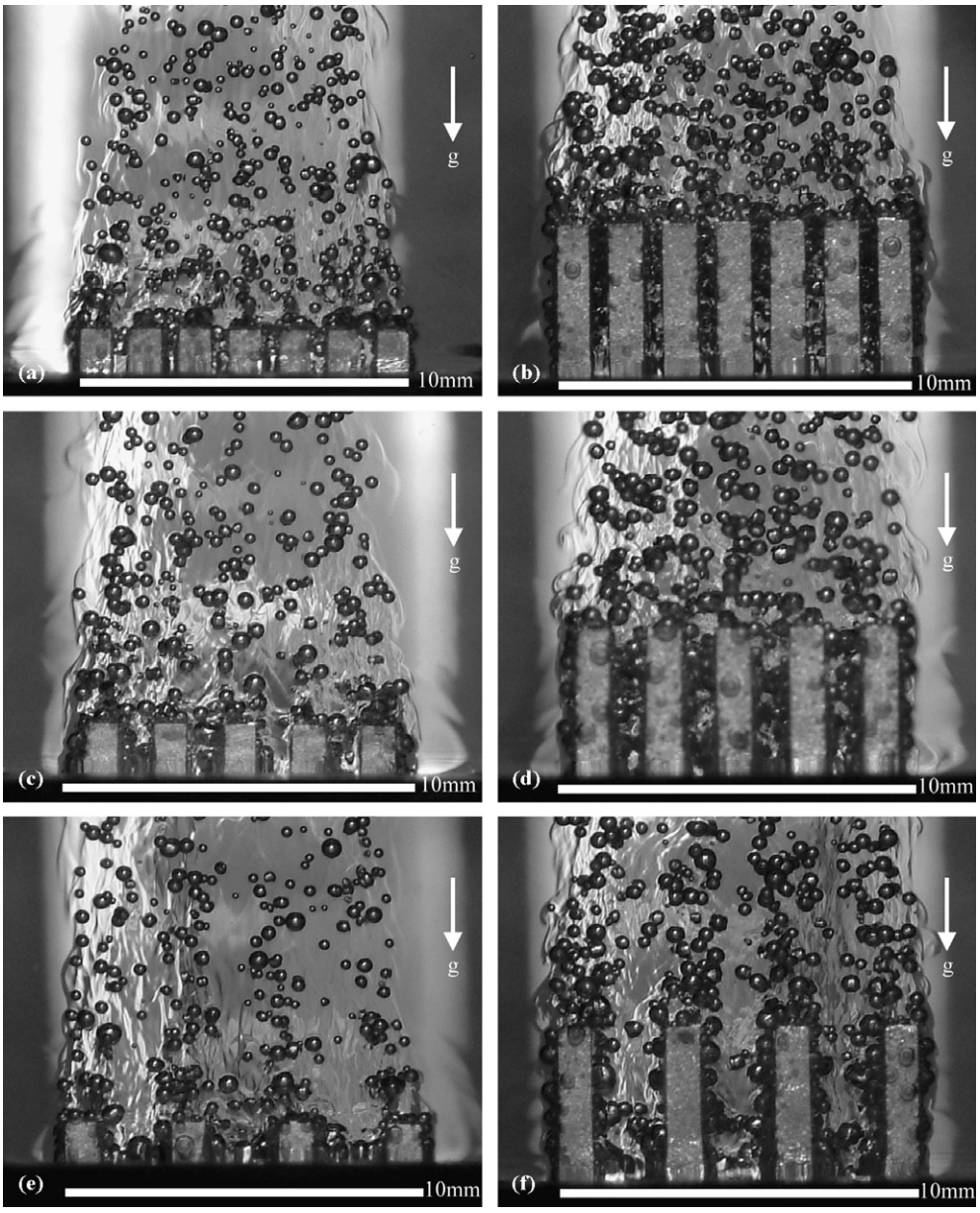

Fig. 5. Flow patterns of 6 finned surfaces at moderate heat flux region. (a) $S = 0.5$ mm, $L = 1.0$ mm, 56.1% of CHF; (b) $S = 0.5$ mm, $L = 4.0$ mm, 56.8% of CHF; (c) $S = 1.0$ mm, $L = 1.0$ mm, 56.1% of CHF; (d) $S = 1.0$ mm, $L = 4.0$ mm, 57.3% of CHF; (e) $S = 2.0$ mm, $L = 1.0$ mm, 57.4% of CHF; (f) $S = 2.0$ mm, $L = 4.0$ mm, 58.3% of CHF.

$$Ja = \left(\frac{\rho_l C p_l \Delta T_{sat}}{\rho_g i_{fg}} \right) \tag{9}$$

For the dielectric FC-72 fluid tested under atmospheric condition, the departure diameter is estimated to be around 0.2–0.3 mm. The estimated bubble departure diameter was verified by observation herein and that by Rini et al. [24]. For another dielectric fluid, HFE7100, a corresponding value of 0.55 mm was obtained by EL-Genk et al. [25].

Fig. 4 shows that the number of active nucleate sites and the bubble departure frequency increased with a small rise in heat flux. The boiling regions gradually spread from the fin tip to the fin root. The figures also indicate that some bubbles began to impact the adjacent fin and activate the non-active cavities thereon. Moreover, the flow patterns showed that active nucleate cavities maintain distinctly and bubbles departure without interaction in inferior heat flux region. The departure bubble diameter observed herein were still maintains at 0.2–0.3 mm.

The flow patterns displayed in Fig. 5 are obtained from six different finned surfaces boiling in the moderate heat flux region. The figures reveal a sharp rise in nucleation density and departure frequency. In Fig. 5a–d, large number of bubbles generated from side surfaces of fins and also result entire fin surfaces covered with growth bubbles. Moreover, bubbles generated from the side surface of fins

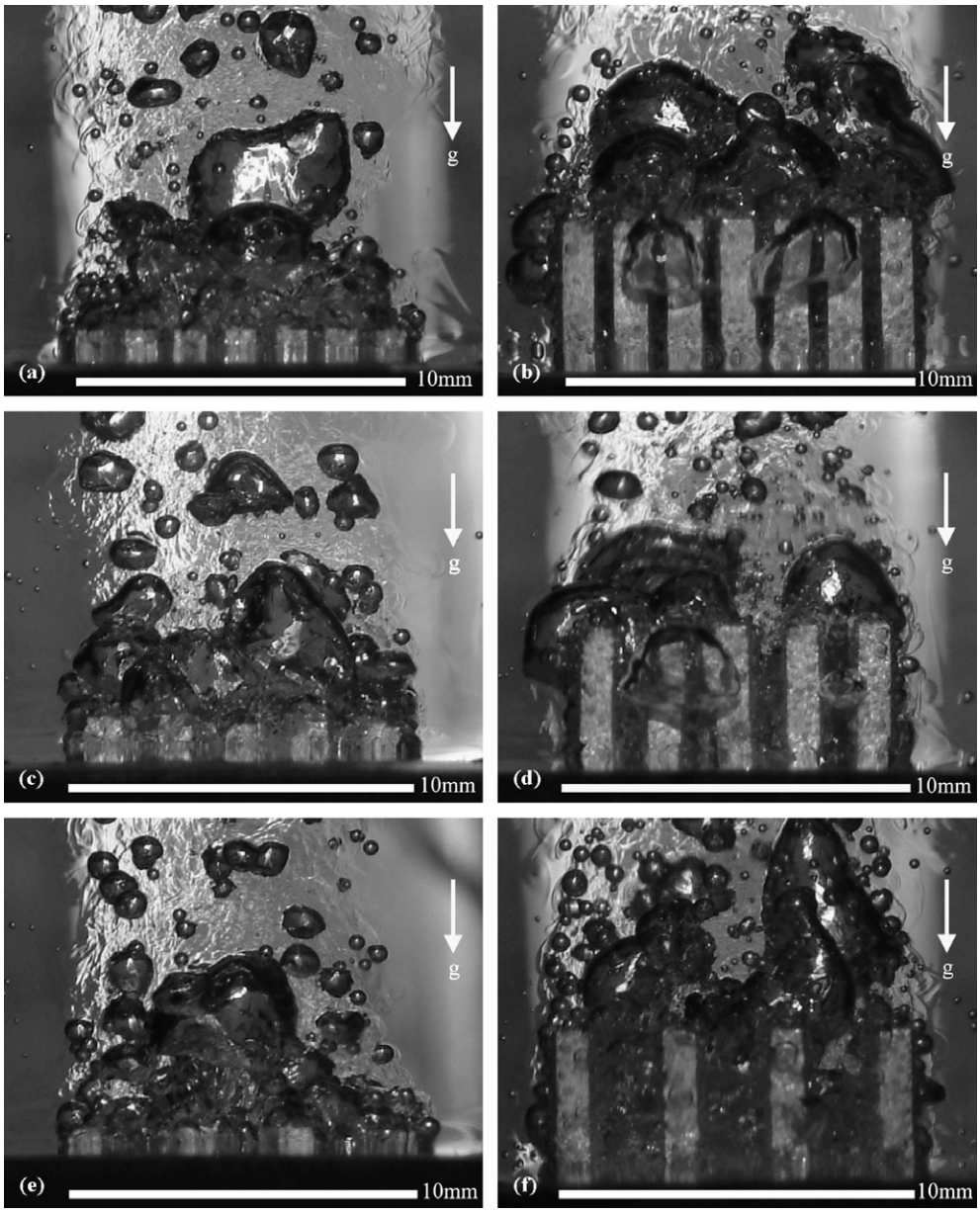

Fig. 6. Flow patterns of 6 finned surfaces at high heat flux region approach to CHF. (a) $S = 0.5$ mm, $L = 0.5$ mm, 84.7% of CHF; (b) $S = 0.5$ mm, $L = 4.0$ mm, 81.3% of CHF; (c) $S = 1.0$ mm, $L = 0.5$ mm, 82.7% of CHF; (d) $S = 1.0$ mm, $L = 4.0$ mm, 84.9% of CHF; (e) $S = 2.0$ mm, $L = 0.5$ mm, 84.5% of CHF; (f) $S = 2.0$ mm, $L = 4.0$ mm, 83.8% of CHF.

began to detach from or slid along the fin. The interactions and coalescence of bubbles were also observed in the closer spacing between adjacent fins. These mechanisms inducing flow resistance to against the lift-off bubbles along the fin. Flow resistance also delays the departure bubbles generated from the fin root and causes the bubbles to coalesce inside fin spacing during the longer lift-off time. Fig. 5e and f present the flow patterns of the surface with the fins more widely spaced $S = 2$ mm. Unlike the compacter fin array in which bubbles interfere with each other inside fin spacing, the boiling mechanisms of rarer fin array are more similar to those on the isolated fin. The departure bubble diameter observed herein range from 0.3 to 0.5 mm.

When the heat flux approached to CHF (seen from Fig. 6), a short periodical departure flow process was investigated, and large vapor mushroom clouds were found to accumulate inside the fin spacing, before splitting into several vapor clouds prior to lift-off. In Fig. 6b and d, larger flow resistance along the narrower spacing and longer fin length result parts of vapor mushroom clouds extruded from the perimeter of the fin array. This periodical departure process may have obstructed and delay the re-wetting liquid entering the fin array, finally causing temporary dry-out in the center of the fin array and rapid rising the wall superheat, leading to critical heat flux.

8. The effects of the geometry parameter on boiling incipience wall superheat and CHF

The boiling incipience wall superheat and CHF value of the finned surfaces with various fin spacing are schematically depicted in Fig. 7a–c. The figures plot the conventional boiling curves (q''_b vs. ΔT) with increasing heat flux. The test result obtained from plain surface was also plotted for comparison. The data indicated that, for all finned surfaces, the boiling incipience wall superheat were approximately 7–11 K and the temperature excursions of hysteresis were about 1–3 K. The boiling hysteresis wall superheat of finned surfaces was obviously less than that of the plain surface (27.32 K). Table 3 presents the boiling incipience wall superheat with various fin spacing and lengths. The boiling incipience wall superheat decreased as the fin length increased or fin spacing decreased, because of the much larger fin surface area the more nucleate sites. Moreover, the temperature overshoot was also eliminated with the compact finned surface.

Table 3
Boiling incipience wall superheat of finned surfaces

Boiling incipience wall superheat (K)	$L = 0.5$ mm	$L = 1.0$ mm	$L = 2.0$ mm	$L = 4.0$ mm
$S = 0.5$ mm	10.49	8.37	8.05	7.62
$S = 1.0$ mm	10.71	8.50	8.36	8.23
$S = 2.0$ mm	11.25	10.22	9.52	9.10

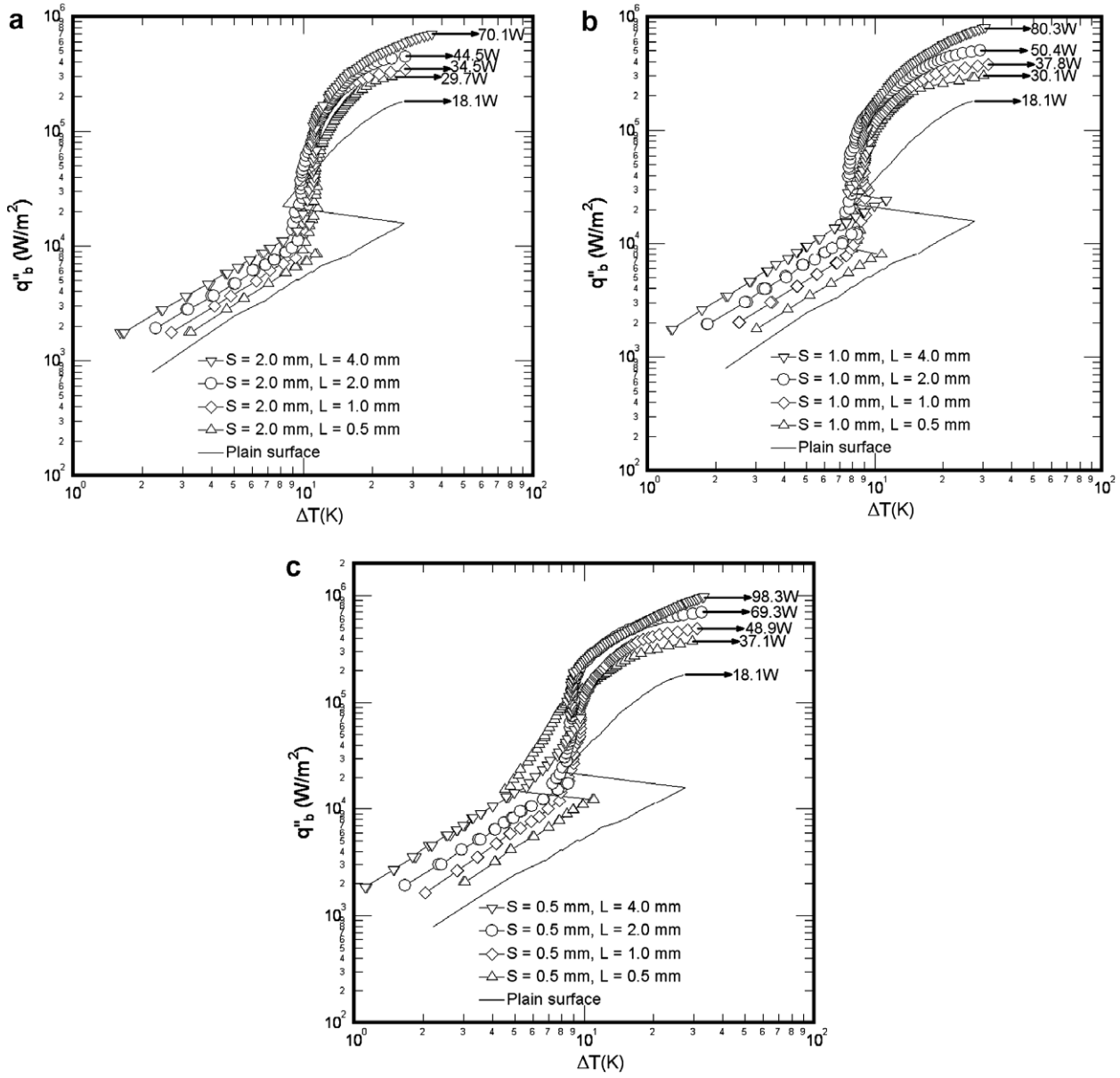

Fig. 7. Boiling curves of copper finned surface with increasing heat flux. (a) Finned surfaces of 2 mm fin spacing, (b) finned surfaces of 1 mm fin spacing and (c) finned surfaces of 0.5 mm fin spacing.

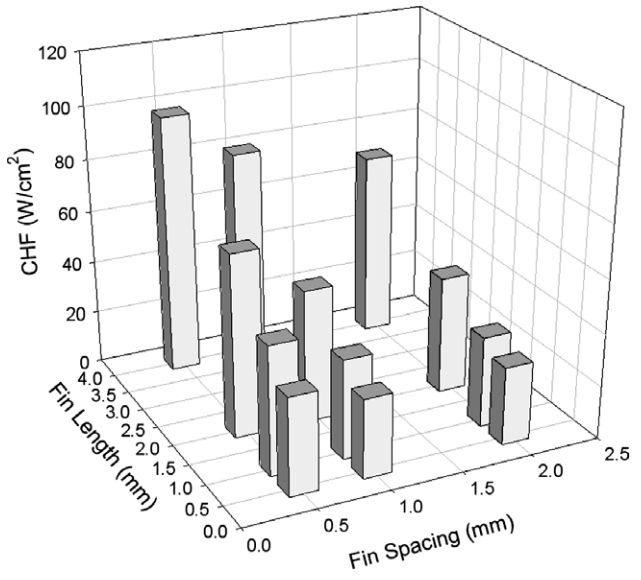

Fig. 8. Critical heat flux varied with fin spacing and length.

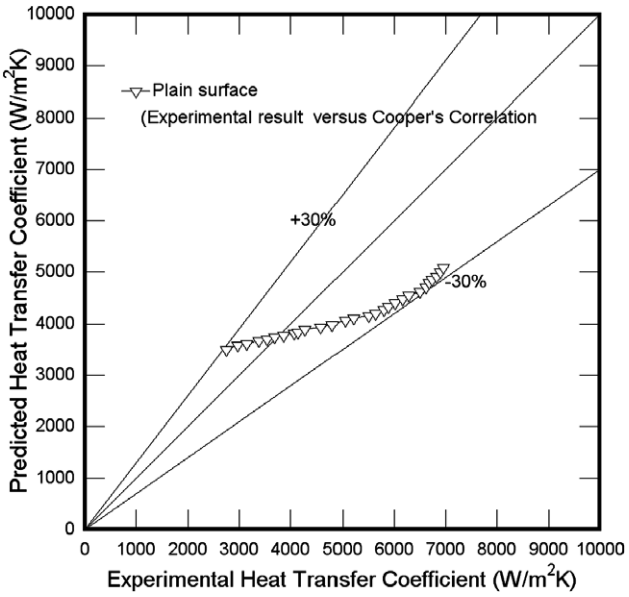

Fig. 9. Experimental result of plain surface versus Cooper's correlation.

As the boiling is initiated, the bubbles were generated from some locations of the finned surface and a large portion of the surface is still in the natural convection condition. When the boiling regions spread, the temperature excursion of wall superheat was constantly occurred and result boiling curve show a vibrating behavior on wall superheat, which is different from the plain surface. Hence, compared with the high hysteresis of the plain surface, the boiling hysteresis of the finned surfaces were relatively indistinct. Until the entire surface was in boiling condition, the superheat eventually increased with the heat flux.

The CHF value (q''_b) varies with the geometry of the structure as presented in Fig. 8, which plots versus fin spacing and fin length. Increasing the heat transfer area per unit base surface increasing heat dissipation, as occur when the fins are closer or the higher. The decrease in the fin spacing indicated the increase in the numbers of fins and the wetting area. The increase in fin length also can increase the wetting area. Hence, the closer fins (more compact fin array) and higher fins can provide more wetting area for boiling.

9. The effects of the geometry parameter on heat transfer

The test results for a plain surface in present study were compared with the well-know plain configuration and those predicted by Cooper [26] in Fig. 9. The Cooper's correlation is given as

$$h_0 = 55(q'')^{0.67}M^{-0.5}Pr^{m}(-\log_{10}Pr)^{-0.55} \quad (10)$$

$$m = 0.12 - 0.2\log_{10}R_p \quad (11)$$

As reported by Stephan and Abdelsalam [27], the commercially finished copper tubes generally have a surface roughness of 0.4 μm. Therefore, the surface roughness, R_p, is given as 0.4 μm in the this calculation. The surface roughness, R_p, only slightly affects the rate of heat transfer, as demonstrated by Cooper [26]. Predictions made using the Cooper correlation typically are fairly consistent with data herein. Fig. 9 reveals that the test data are within −30/+30% of the results obtained using Cooper correlation. The experimental data indicated that for $q''_b > 3 \times 10^4\ W\ m^{-2}$ the predictions by the Cooper correlation over-predicts the present test results for all the test refrigerants. This is attributed to the Cooper correlation gave a fixed exponent (0.67) dependence of heat flux.

The plots presented in Fig. 10a–c illustrated the changes of overall boiling heat transfer coefficient on copper finned surfaces with overall heat flux for various fin spacing and lengths. At a larger fin spacing of $S = 2$ mm shown in Fig. 10a, the slopes of the boiling curves are approximately the same in the region $q''_t < 5 \times 10^4\ W\ m^{-2}$, independently of the lengths of the fins. However, greater fin lengths yield lower overall heat transfer coefficients in moderate and high heat flux regions that $q''_t > 5 \times 10^4\ W\ m^{-2}$. It is obviously due to the effect of flow resistance to departure bubble and superheated liquid increased with the fin length. The photo images in Fig. 5e indicated that bubbles either lift-off directly from the fin tip and base surface or slide for a short distance along the fins. However, for the higher fin arrangements observed in Fig. 5f, large number of bubbles generated from the side surfaces of fins and slide along the fins before detach from the fins. Those sliding bubbles might obstruct the lift-off bubble departed from the fin root and base surface. Similar behavior was more noticeable in smaller spacing of $S = 0.5$ mm and $S = 1$ mm that shown in Fig. 5b and d. Therefore, at a smaller fin spacing of $S = 0.5$ mm, as shown in Fig. 10c, the slopes of the boiling curves changed considerably with the fin length in the region $q''_t > 1.6 \times 10^4\ W\ m^{-2}$. The results further verified that increase the fin length or decrease the fin spacing increase the resistance against bubble departure.

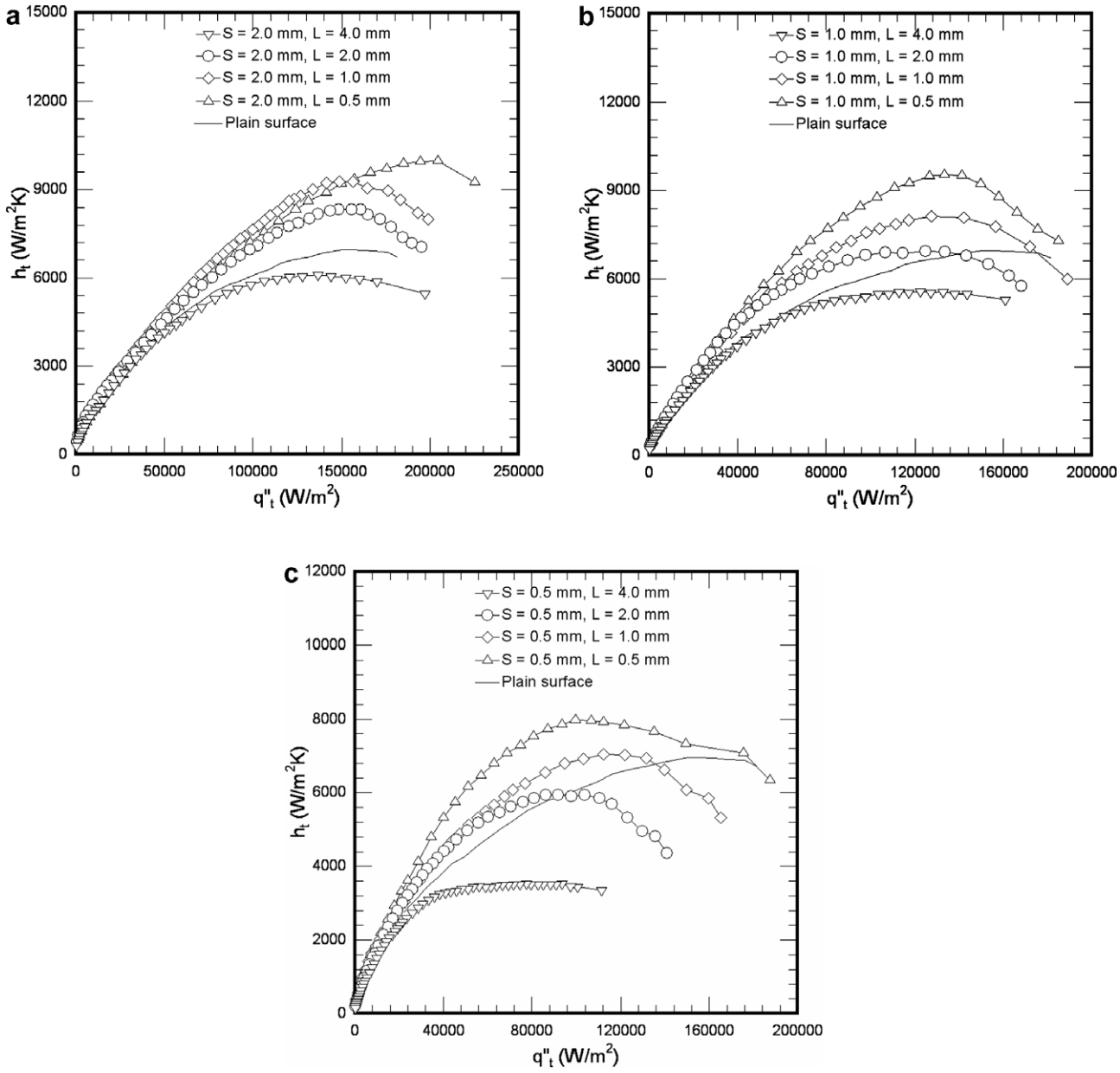

Fig. 10. The changes of overall boiling heat transfer coefficient on copper finned surfaces with overall heat flux for various fin spacing and lengths. (Decreasing heat flux). (a) Finned surfaces of 2 mm fin spacing, (b) finned surfaces of 1 mm fin spacing and (c) finned surfaces of 0.5 mm fin spacing.

The plots in Fig. 10a–c also demonstrated, at low heat fluxes of below around 3×10^4 W m^{-2}, the boiling curve of all test surfaces varied similarly with heat flux except the cases of $L = 4$ mm. As the heat flux was increased, the overall heat transfer coefficients of most finned surfaces increased to a maximum value, before decreasing as the heat flux was increased further. This behavior can be explained by the increase in the active nucleate density as the wall temperature rises, until large clusters and accumulations of vapor form among the fins. After the peak value, the overall heat transfer coefficients began to decay because of the increase in departure bubble resistance. However, the case with $L = 4$ mm in Fig. 10 b and c behaved differently and its overall heat transfer coefficient was independent of heat flux. As describe of above flow pattern observation, this behavior may be cause by the suppression of departure bubble by long fin length. Moreover, the premature decline in overall heat transfer coefficients was noted in Fig. 10a and c for high fin length arrangements, and similar trend was also observed by Guglielmini [9] and Rainey [11].

It was also note that all curves in Fig. 10 have almost the same overall heat transfer coefficients in low heat flux region. Fig. 11 re-plot the overall heat transfer coefficients versus the overall heat flux for twelve test surfaces that before overall heat transfer coefficient began to decline or

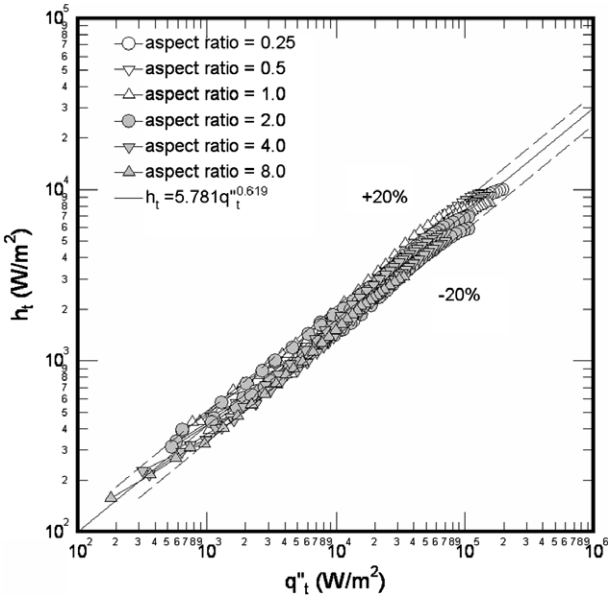

Fig. 11. Overall heat transfer coefficients versus overall heat flux for different finned surfaces.

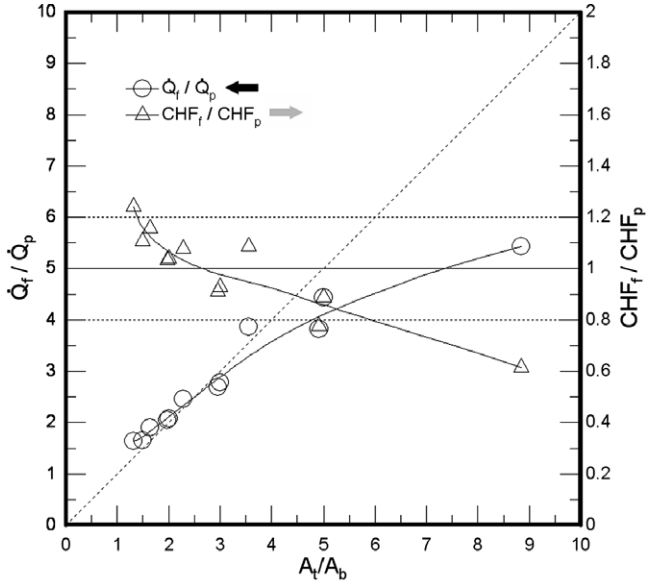

Fig. 12. Enhancement of critical heat flux versus enhancement of area.

level-off. The plots in Fig. 11 showed that all experimental data lie on a straight line which can be correlated a linear equation in the following form:

$$h_t = 5.781 q_t''^{0.619} \tag{12}$$

Eq. (12) can also be written in term of power law

$$q_t'' = 100 \Delta T^{2.625} \tag{13}$$

10. Relationship between CHF ratio, area ratio and aspect ratio

Fig. 12 plots the enhance heat transfer ratio ($\dot{Q}_f/\dot{Q}_p$) versus the area ratio (A_t/A_b). The figure shows that $\dot{Q}_f/\dot{Q}_p$ increased with A_t/A_b, so increasing the area increased the heat transfer. However, the plot also showed that $\dot{Q}_f/\dot{Q}_p$ was not always proportional to A_t/A_b, but that $\dot{Q}_f/\dot{Q}_p$ increased as A_t/A_b decreased. In response of large increase in area, the enhancement of heat transfer rate decreased because increasing the area by increasing fin length or making fin closer increased flow resistance to departure vapor mushrooms.

Fig. 12 also plotted CHF_f/CHF_p against A_t/A_b. It shows two distinct regions of enhancements – $CHF_t/CHF_p < 1$ and $CHF_t/CHF_p > 1$. A comparison with Table 1 shows that the plot of CHF_f/CHF_p corresponded to the fin aspect ratio (fin length versus fin spacing). In the region $CHF_t/CHF_p > 1$, the fin aspect ratio of the test surfaces were all less than or equal to 1. In the region in which $CHF_t/CHF_p < 1$, the fin aspect ratios all exceeded 1. Those results prove the flow pattern observation that lower aspect ratio fins, either lower fin length or larger fin spacing, provide lower resistance to the departure bubble and re-wetting liquid and yield higher heat transfer rate per unit area. The above analysis clearly shows that the fin aspect ratio strongly affects the CHF enhancement.

11. Conclusion

Pool boiling on plain and finned surfaces immersed in saturated FC-72 at atmospheric pressure was experimentally studied. The effects of geometry parameters on the nucleate boiling heat transfer performance with fins of various lengths and spacing were also reported. The experimental results support the following conclusions:

(1) Boiling generally initiated at the tip of the fin, whence it spread to the fin root, regardless the wall superheat at the fin root exceeded that of the fin tip. This result was associated with the fact that generated bubbles can be easily trapped at the fin root and eliminated by the convective flow.
(2) A short periodical departure flow process was investigated as heat flux approach to the CHF, and large vapor mushroom clouds were found to accumulate inside the fin spacing, before splitting into several vapor clouds prior to lift-off.
(3) Boiling incipience wall superheat decreased as the fin length increases and the fin spacing decreases. The denser and higher fin array also eliminated the temperature overshoot. Reducing the fin spacing and increasing the fin length also increased the flow resistance to bubble departure and also caused an early decline or level-off of the overall heat transfer coefficient.
(4) Reducing the fin spacing or increasing the fin length can raise the heat transfer rate. The maximum heat transfer rate of the test surface with the smallest fin spacing and the highest fins was 98.3 W, which almost five times that of the plain surface.

(5) The enhancement of heat transfer rate was not proportional to the total area enhancement of the finned surface. Lower aspect ratio fins, either lower fin length or larger fin spacing, provide lower resistance to the departure bubble and re-wetting liquid and yield higher heat transfer rate per unit area.

References

[1] A. Bar-Cohen, State-of-the-art and trends in the thermal packaging of electronic equipment, ASME J. Electron. Pack. 114 (1992) 254–270.

[2] J.R. Thome, Enhanced Boiling Heat Transfer, Hemisphere, New York, 1990.

[3] D.L. Bondurant, J.W. Westwater, Performance of transverse fins for boiling heat transfer, Chem. Eng. Sci. 20 (1) (1971) 837–849.

[4] G.J. Klein, J.W. Westwater, Heat transfer from multiple spines to boiling liquids, AIChE J. 17 (5) (1971) 1050–1056.

[5] K.W. Haley, J.W. Westwater, Boiling heat transfer from a single fins, in: Proceedings of the 3rd International Heat Transfer Conference, vol. 3, Chicago, (1966) pp. 245–253.

[6] I. Mudawar, T.M. Anderson, Optimization of enhanced surfaces for high flux chip cooling by pool boiling, ASME J. Electron. Pack. 115 (1993) 89–100.

[7] M. Siman-Tov. Analysis and design of extended surfaces in boiling liquids, in: Chem. Engrg. Progr. Symp. Ser. 66 (1970) pp. 174–184.

[8] G. Guglielmini, M. Misale, C. Schenone, Experiments on Pool Boiling of a Dielectric Fluid on Extended Surfaces, Int. Commun. Heat Mass Transf. 23 (4) (1996) 451–462.

[9] G. Guglielmini, M. Misale, C. Schenone, Boiling of saturated FC-72 on square pin fin arrays, Int. J. Therm. Sci. 41 (2002) 599–608.

[10] J.Y. Chang, S.M. You, Boiling heat transfer phenomena from microporous and porous surfaces in saturated FC-72, Int. J. Heat Mass Transf. 40 (18) (1997) 4437–4447.

[11] K.N. Rainey, S.M. You, Pool boiling heat transfer from plain and microporous, square pin-finned surfaces in saturated FC-72, ASME J. Heat Transf. 122 (2000) 509–516.

[12] Y. Hirono, R. Shimada, S. Kumagai, K. Kaino, T. Takeyama, Optimization of fin array in boiling heat transfer, technical report, Tohoku University, 50(1), 1985, pp. 21–39.

[13] L. Zhang, M. Shoji, Nucleation site interaction in pool boiling on the artificial surface, Int. J. Heat Mass Transf. 46 (2003) 513–522.

[14] M. Shoji, Y. Takagi, Bubbling features from a single artificial cavity, Int. J. Heat Mass Transf. 44 (2001) 2763–2776.

[15] H. Honda, J.J. Wei, Effects of fin geometry on boiling heat transfer from silicon chips with micro-pin-fins immersed in FC-72, Int. J. Heat Mass Transf. 46 (21) (2003) 4059–4070.

[16] C.K. Yu, D.C. Lu, T.C. Cheng, Pool boiling heat transfer on artificial micro-cavity surfaces in dielectric fluid FC-72, J. Micromech. Microeng. 16 (2006) 2092–2099.

[17] W. Nakayama, T. Daikoku, H. Kuwahara, T. Nakajima, Dynamic model of enhanced boiling heat transfer on porous surfaces Part I: experimental investigation, J. Heat Transf. 102 (1980) 445–450.

[18] W. Nakayama, T. Daikoku, H. Kuwahara, T. Nakajima, Dynamic model of enhanced boiling heat transfer on porous surfaces Part II: analytical modeling, J. Heat Transf. 102 (1980) 451–456.

[19] W. Nakayama, T. Daikoku, T. Nakajima, Effects of pore diameters and system pressure on saturated pool boiling heat transfer from porous surfaces, J. Heat Transf. 104 (1982) 286–291.

[20] J. Arshad, J.R. Thome, Enhanced boiling surfaces: heat transfer mechanism and mixture boiling, in: Proceedings of 1ASME-JSME Thermal Engineering Joint Conference, 1(1), 1983, pp. 191–197.

[21] C. Xia, Weilin. Hu, Z. Guo, Natural convective boiling in vertical rectangular narrow channels, Exp. Therm Fluid Sci. 12 (1996) 313–324.

[22] S.J. Kline, F.A. Mcclintock, Describing the uncertainties in single-sample experiment, Mech. Eng. 75 (1) (1953) 3–12.

[23] R. Cole, Bubble frequencies and departure volumes at subatomosheric pressures, AIChE J. 13 (1967) 779–783.

[24] D. Rini, R. Chen, L. Chow, Bubble behavior and heat transfer mechanism in FC-72 boiling, Exp Heat Transf. 14 (2001) 27–44.

[25] M.S. EL-Genk, H. Bostanci, Saturation Boiling of HFE-7100 from A Copper Surface, Saturation boiling of HFE-7100 from a copper simulating surface a microelectronic chip, Int. J. Heat Mass Transf. 46 (2003) 1841–1854.

[26] M.G. Cooper. Saturation nucleate pool boiling – a simple correlation, 31st U.K. national conference on heat transfer, in: International Chemical Engineering Symposium Series 86 (1984) pp. 785–792.

[27] K. Stephan, M. Abdelsalam, Heat transfer correlations for natural convection boiling, Int. J. Heat Mass Transf. 23 (1980) 73–87.